5 Quantum Monte Carlo Impurity Solvers

Philipp Werner
University of Fribourg
Chemin du Musée 3, 1700 Fribourg, Switzerland

Contents

1 Quantum impurity models **2**
1.1 Action formulation . . . 3
1.2 Dynamical mean-field theory . . . 4

2 Continuous-time QMC solvers – General formalism **6**

3 Weak-coupling approach **7**
3.1 Sampling . . . 9
3.2 Determinant ratios and fast matrix updates . . . 10
3.3 Measurement of the Green function . . . 11
3.4 Multi-orbital and cluster impurity problems . . . 12

4 Hybridization-expansion approach **12**
4.1 Sampling . . . 14
4.2 Measurement of the Green function . . . 15
4.3 Generalizations – Matrix and Krylov formalisms . . . 17

5 Scaling of the algorithms **20**

6 Electron-boson systems **23**
6.1 Local phonons . . . 23
6.2 Frequency-dependent interactions . . . 26
6.3 Boson distribution function . . . 27

E. Pavarini, E. Koch, A. Lichtenstein, and D. Vollhardt (eds.)
Dynamical Mean-Field Theory of Correlated Electrons
Modeling and Simulation Vol. 12
Forschungszentrum Jülich, 2022, ISBN 978-3-95806-619-9
http://www.cond-mat.de/events/correl22

1 Quantum impurity models

A quantum impurity model describes an atom or molecule embedded in some host with which it exchanges electrons or spin. This exchange allows the impurity to make transitions between different quantum states, and these transitions lead to non-trivial dynamical properties. Quantum impurity models play a prominent role, for example, in the theoretical description of dilute metal alloys and in theoretical studies of quantum dots and molecular conductors. These models also appear as an auxiliary problem whose solution yields the dynamical mean-field description of correlated lattice models.
The Hamiltonian of a general impurity model has the form

$$H = H_{\rm loc} + H_{\rm bath} + H_{\rm mix}, \tag{1}$$

where $H_{\rm loc}$ describes the impurity, characterized by a small number of degrees of freedom (typically spin and orbital degrees of freedom denoted by a, b, ...), and $H_{\rm bath}$ describes an infinite reservoir of free electrons, labeled by a continuum of quantum numbers p and a discrete set of quantum numbers ν (typically spin). $H_{\rm mix}$ describes the exchange of electrons between the impurity and the bath in terms of hybridization amplitudes $V^a_{p\nu}$. Denoting the impurity creation operators by $d^\dagger$ and the bath creation operators by $c^\dagger$, the three terms are

$$\begin{aligned} H_{\rm loc} &= \sum_{ab} \epsilon^{ab} d^\dagger_a d_b + \frac{1}{2}\sum_{abcd} U^{abcd} d^\dagger_a d^\dagger_b d_c d_d, & (2)\\ H_{\rm bath} &= \sum_{p\nu} \varepsilon_p c^\dagger_{p\nu} c_{p\nu}, & (3)\\ H_{\rm mix} &= \sum_{pa\nu} \left(V^a_{p\nu}\, d^\dagger_a c_{p\nu} + (V^a_{p\nu})^* c^\dagger_{p\nu} d_a \right). & (4) \end{aligned}$$

In most of the following discussions, we focus on the single-orbital Anderson impurity model, where the local Hamiltonian

$$\begin{aligned} H_{\rm loc} &= H_\mu + H_U, & (5)\\ H_\mu &= -\mu(n_\uparrow + n_\downarrow), & (6)\\ H_U &= U\, n_\uparrow n_\downarrow, & (7) \end{aligned}$$

has a Hilbert space of dimension four. The discrete quantum number labeling the impurity states is the spin σ, $n_\sigma = d^\dagger_\sigma d_\sigma$ is the density operator for impurity electrons with spin σ, and the chemical potential is $\mu = -\epsilon$. The bath and mixing terms are

$$\begin{aligned} H_{\rm bath} &= \sum_{p\sigma} \varepsilon_p c^\dagger_{p\sigma} c_{p\sigma}, & (8)\\ H_{\rm mix} &= \sum_{p\sigma} \left(V_{p\sigma}\, d^\dagger_\sigma c_{p\sigma} + V^*_{p\sigma} c^\dagger_{p\sigma} d_\sigma \right). & (9) \end{aligned}$$

An illustration of the Anderson impurity model is shown in Fig. 1.

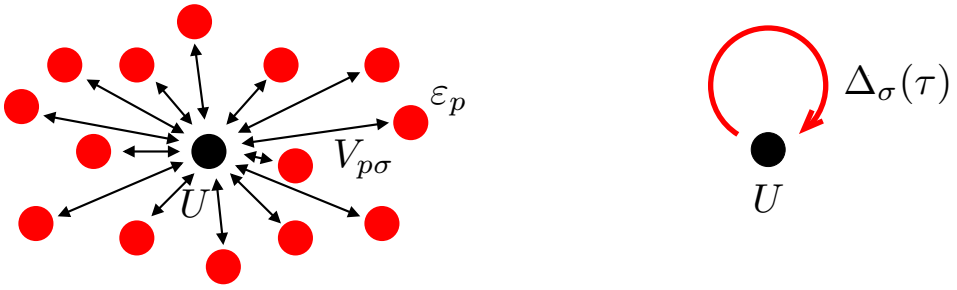

Fig. 1: *Schematic representation of the Anderson impurity model. The left panel illustrates the Hamiltonian representation. Spin up and down electrons on the impurity (black dot) interact with an on-site energy U and hop to a continuum of non-interacting bath levels with energy ε_p. The amplitudes for these transitions are given by the hybridization parameters $V_{p\sigma}$. Right panel: Action representation of the Anderson impurity model, where the bath is replaced by the hybridization function $\Delta_\sigma(\tau)$.*

1.1 Action formulation

For analytical and numerical studies of equilibrium impurity problems, it can be useful to express the partition function and the imaginary-time Green function in terms of the imaginary-time action. By integrating out the bath degrees of freedom in the path integral formalism one obtains the partition function of the Anderson impurity model as

$$Z = \mathrm{Tr}_d\big(\mathcal{T} e^{-S}\big),$$

with the impurity action $S = S_{\mathrm{mix}} + S_{\mathrm{loc}}$ given by

$$S_{\mathrm{mix}} = \sum_\sigma \int_0^\beta d\tau d\tau'\, d^\dagger_\sigma(\tau')\Delta^\sigma(\tau'-\tau)d_\sigma(\tau), \tag{10}$$

$$S_{\mathrm{loc}} = \int_0^\beta d\tau \Big(-\mu\big(n_\uparrow(\tau)+n_\downarrow(\tau)\big) + U\, n_\uparrow(\tau)n_\downarrow(\tau)\Big). \tag{11}$$

$\mathcal{T}$ is the time-ordering operator. The impurity Green function becomes

$$G(\tau) = -\big\langle \mathcal{T} d(\tau)d^\dagger(0)\big\rangle_S = -\frac{1}{Z}\mathrm{Tr}_d\big(\mathcal{T} e^{-S} d(\tau)d^\dagger(0)\big).$$

The imaginary-time and Matsubara-frequency representations are related by

$$G(i\omega_n) = \int_0^\beta d\tau\, e^{i\omega_n\tau} G(\tau), \qquad G(\tau) = \frac{1}{\beta}\sum_n e^{-i\omega_n\tau} G(i\omega_n),$$

where the fermionic Matsubara frequencies are $\omega_n = (2n+1)\pi/\beta$ and $\beta = 1/T$ is the inverse temperature.

The hybridization function $\Delta^\sigma(\tau'-\tau)$ in Eq. (10) represents the amplitude for hopping from the impurity into the bath at time τ and back onto the impurity at time τ'. It is a function of the

bath energies and hybridization amplitudes and is most conveniently expressed in Matsubara frequency space:

$$\Delta^\sigma(i\omega_n) = \sum_p \frac{|V_{p\sigma}|^2}{i\omega_n - \varepsilon_p}. \tag{12}$$

It is also useful to introduce the Green function of the non-interacting impurity, $\mathcal{G}_0$, which is related to the hybridization function by

$$[\mathcal{G}_0^\sigma]^{-1}(i\omega_n) = i\omega_n + \mu - \Delta^\sigma(i\omega_n). \tag{13}$$

1.2 Dynamical mean-field theory

Quantum impurity models are a key ingredient of the dynamical mean-field theory (DMFT), which provides an approximate description of correlated lattice models [1]. The success of DMFT created a demand for accurate and versatile impurity solvers and triggered the development of the continuous-time impurity solvers. These solvers have been discussed in detail in various lecture notes [2], reviews [3] and books [4]. Our presentation here follows closely Chapter 8 in Ref. [4].

In this section, we briefly introduce the DMFT approximation, which maps an interacting lattice model, such as the Hubbard model, onto an effective single-site problem (impurity model) subject to a self-consistency condition for the bath.

The Hubbard model

$$H_{\text{Hubbard}} = -t \sum_{\langle ij\rangle\sigma} \left(d^\dagger_{i\sigma} d_{j\sigma} + d^\dagger_{j\sigma} d_{i\sigma}\right) + U \sum_i n_{i\uparrow} n_{i\downarrow} - \mu \sum_{i\sigma} n_{i\sigma}$$

describes electrons hopping between nearest neighbor sites of some lattice with amplitude t. Two electrons on the same site interact with energy U. The chemical potential term has been added because we will work in the grand canonical ensemble. The noninteracting dispersion ϵ_k is obtained as the Fourier transform of the hopping matrix. For example, in the case of a one-dimensional lattice with lattice spacing a, $\epsilon_k = -2t\cos(ka)$.

Inspired by the Weiss molecular-field theory [1], we focus on one particular site of the lattice and replace the remaining degrees of freedom of the model by a bath of non-interacting levels and a hybridization term that connects the interacting site to the bath. The effective single-site problem thus becomes an Anderson impurity model,[1]

$$H_{\text{imp}} = \sum_{p\sigma} \varepsilon_p c^\dagger_{p\sigma} c_{p\sigma} + \sum_{p\sigma} \left(V_{p\sigma} d^\dagger_\sigma c_{p\sigma} + V^*_{p\sigma} c^\dagger_{p\sigma} d_\sigma\right) + U n_\uparrow n_\downarrow - \mu(n_\uparrow + n_\downarrow). \tag{14}$$

Here, the $d^\dagger$ create electrons on the impurity, $n_\sigma = d^\dagger_\sigma d_\sigma$, and the $c^\dagger_p$ create electrons in bath states labeled by a quantum number p. In this effective single-site model, hoppings from the impurity into the bath and back represent processes in the original Hubbard model where an

[1] In the DMFT context, the bath energy levels ε_p of the impurity model are not directly related to the dispersion of the lattice model, ϵ_k.

electron hops from a given site into the lattice and returns to it after some excursion through the lattice. The hybridization parameters V_p give the amplitudes for such processes.

The DMFT procedure optimizes the parameters ε_p and V_p such that the bath of the Anderson impurity model mimics the lattice environment as closely as possible. If we work with the impurity action, the bath properties are encoded in $\Delta(\tau)$ or $\mathcal{G}_0(\tau)$ and these functions thus play the role of the mean field. It is a *dynamical* mean field, because the hybridization function Δ or Weiss Green function $\mathcal{G}_0$ depends on (imaginary) time or frequency.

The self-consistent solution is constructed in such a way that the impurity Green function $G_{\text{imp}}(i\omega_n)$ reproduces the *local* lattice Green function $G_{\text{loc}}(i\omega_n) \equiv G_{i,i}(i\omega_n)$. In other words, if $G(k, i\omega_n)$ is the momentum-dependent lattice Green function of the Hubbard model, we seek bath parameters and hybridizations such that the *DMFT self-consistency condition*

$$\int (dk)\, G(k, i\omega_n) \equiv G_{\text{imp}}(i\omega_n) \tag{15}$$

is satisfied.[2] The solution of Eq. (15) is obtained by iteration. To define a practical procedure, we have to relate the left-hand-side of Eq. (15) to impurity model quantities. This step involves, as the essential approximation of the DMFT method, a significant simplification of the momentum-dependence of the lattice self-energy [5].

The self-energy describes the effect of interactions on the propagation of electrons. In the non-interacting model, the lattice Green function is $G_0(k, i\omega_n) = \left(i\omega_n + \mu - \epsilon_k\right)^{-1}$, with ϵ_k being the Fourier transform of the hopping matrix. The Green function of the interacting model is $G(k, i\omega_n) = \left(i\omega_n + \mu - \epsilon_k - \Sigma(k, i\omega_n)\right)^{-1}$ with $\Sigma(k, i\omega_n)$ the lattice self-energy. Therefore

$$\Sigma(k, i\omega_n) = G_0^{-1}(k, i\omega_n) - G^{-1}(k, i\omega_n).$$

Similarly, we obtain the impurity self-energy

$$\Sigma_{\text{imp}}(i\omega_n) = \mathcal{G}_0^{-1}(i\omega_n) - G_{\text{imp}}^{-1}(i\omega_n),$$

with $\mathcal{G}_0^{-1}$ defined in Eq. (13). The DMFT approximation is the identification of the lattice self-energy with the momentum-independent impurity self-energy,

$$\Sigma(k, i\omega_n) \approx \Sigma_{\text{imp}}(i\omega_n).$$

This approximation allows us to rewrite the self-consistency equation (15) as

$$\int (dk)\, \left(i\omega_n + \mu - \epsilon_k - \Sigma_{\text{imp}}(i\omega_n)\right)^{-1} \equiv G_{\text{imp}}(i\omega_n). \tag{16}$$

Since both $G_{\text{imp}}(i\omega_n)$ and $\Sigma_{\text{imp}}(i\omega_n)$ are determined by the impurity model parameters ε_p and V_p (or the function $\Delta(\tau)$ or $\mathcal{G}_0(\tau)$), Eq. (16) defines a self-consistency condition for these parameters (or functions).

We now formulate the self-consistency loop for the Weiss Green function $\mathcal{G}_0(i\omega_n)$. Starting from an arbitrary initial $\mathcal{G}_0(i\omega_n)$, for example, the local Green function of the noninteracting lattice model, we iterate the following steps until convergence:

[2] $\int (dk)$ denotes a normalized integral over the Brillouin zone.

1. Solve the impurity problem, that is, compute the impurity Green function $G_{\rm imp}(i\omega_n)$ for the given $\mathcal{G}_0(i\omega_n)$,

2. Extract the self-energy of the impurity model: $\Sigma_{\rm imp}(i\omega_n) = \mathcal{G}_0^{-1}(i\omega_n) - G_{\rm imp}^{-1}(i\omega_n)$,

3. Identify the lattice self-energy with the impurity self-energy, $\Sigma(k, i\omega_n) = \Sigma_{\rm imp}(i\omega_n)$ (DMFT approximation), and compute the local lattice Green function:

$$G_{\rm loc}(i\omega_n) = \int (dk) \big(i\omega_n + \mu - \epsilon_k - \Sigma_{\rm imp}(i\omega_n) \big)^{-1},$$

4. Apply the DMFT self-consistency condition, $G_{\rm loc}(i\omega_n) = G_{\rm imp}(i\omega_n)$, and use it to define a new Weiss Green function $\mathcal{G}_0^{-1}(i\omega_n) = G_{\rm loc}^{-1}(i\omega_n) + \Sigma_{\rm imp}(i\omega_n)$.

The computationally expensive step is the solution of the impurity problem (Step 1). When the loop converges, the bath contains information about the lattice (through the density of states), and about the phase (metal, Mott insulator, antiferromagnetic insulator, ...). The impurity, which exchanges electrons with the bath, thus feels, at least to some extent, as if it were a site of the lattice.

2 Continuous-time QMC solvers – General formalism

Quantum impurity models are (0+1)-dimensional quantum field theories and as such are computationally much more tractable than interacting lattice models. The main objective is computing the impurity Green function

$$G(\tau) = -\langle \mathcal{T} d(\tau) d^\dagger(0) \rangle = -\frac{1}{Z} \mathrm{Tr} \Big(e^{-(\beta-\tau)H} d\, e^{-\tau H} d^\dagger \Big), \tag{17}$$

where $Z = \mathrm{Tr}\, e^{-\beta H}$ is the impurity model partition function, β the inverse temperature, $\mathcal{T}$ is the (imaginary) time-ordering operator, and $\mathrm{Tr} = \mathrm{Tr}_d \mathrm{Tr}_c$ the trace over the impurity and bath states. In the last expression we assumed that $0 \le \tau < \beta$.

Continuous-time Monte Carlo algorithms expand the partition function into a series of "diagrams" and stochastically sample these diagrams [3]. We represent the partition function as a sum (or more precisely as an integral) over configurations C with weight w_C,

$$Z = \sum_C w_C, \tag{18}$$

and implement a random walk $C_1 \to C_2 \to C_3 \to \cdots$ in configuration space in such a way that ergodicity and detailed balance are satisfied. Using sign-weighted averages, the impurity Green function can be estimated from a finite number M of measurements as

$$G = \sum_C \frac{w_C\, G_C}{Z} = \frac{\sum_C |w_C| \,\mathrm{sign}_C\, G_C}{\sum_C |w_C| \,\mathrm{sign}_C} \approx \frac{\sum_{i=1}^M \mathrm{sign}_{C_i} G_{C_i}}{\sum_{i=1}^M \mathrm{sign}_{C_i}} \equiv \frac{\langle \mathrm{sign} \cdot G \rangle_{\rm MC}}{\langle \mathrm{sign} \rangle_{\rm MC}}. \tag{19}$$

To derive the general framework for the continuous-time solvers it is useful to express the partition function as an imaginary-time ordered exponential in an *interaction representation*. To do this, we split the Hamiltonian into two parts, $H = H_1 + H_2$, and define the imaginary-time dependent operators in the interaction representation as $O(\tau) = e^{\tau H_1} O e^{-\tau H_1}$. In this representation, the partition function becomes $Z = \mathrm{Tr}\big(e^{-\beta H_1}\mathcal{T} e^{-\int_0^\beta d\tau H_2(\tau)}\big)$.[3]
Next, we expand the time-ordered exponential into a power series,

$$Z = \sum_{n=0}^{\infty} \int_0^\beta d\tau_1 \cdots \int_{\tau_{n-1}}^\beta d\tau_n \,\mathrm{Tr}\,\Big(e^{-(\beta-\tau_n)H_1}(-H_2)\cdots e^{-(\tau_2-\tau_1)H_1}(-H_2)e^{-\tau_1 H_1}\Big). \qquad (20)$$

This yields a representation of the partition function of the form (18), namely, as an infinite sum over the weights of certain configurations. The configurations are collections of time-points on the imaginary-time interval: $C = \{\tau_1, \ldots, \tau_n\}$, $n = 0, 1, \ldots$, where we assume the imaginary-time ordering $\tau_i < \tau_{i+1}$ and the restriction $\tau_i \in [0, \beta)$. The expression for the Monte Carlo weights is

$$w_C = \mathrm{Tr}\Big(e^{-(\beta-\tau_n)H_1}(-H_2)\cdots e^{-(\tau_2-\tau_1)H_1}(-H_2)e^{-\tau_1 H_1}\Big)(d\tau)^n. \qquad (21)$$

There are two complementary continuous-time Monte Carlo techniques: (i) the *weak-coupling approach*, which scales favorably with system size (that is, the number of correlated sites or orbitals in the impurity model) and allows the efficient simulation of relatively large impurity clusters with simple interactions, and (ii) the *hybridization-expansion approach*, which can handle impurity models with strong interactions among multiple orbitals. For simplicity, we continue to focus on the single-orbital Anderson impurity model defined in Eqs. (6)–(9). In this case, the weak-coupling continuous-time Monte Carlo approach expands Z in powers of the interaction U in an interaction representation where the imaginary-time evolution is determined by the *quadratic* part $H_\mu + H_{\mathrm{bath}} + H_{\mathrm{mix}}$ of the Hamiltonian. The complementary hybridization-expansion approach expands Z in powers of the impurity-bath hybridization term H_{mix} in an interaction representation where the imaginary-time evolution is determined by the *local* part $H_\mu + H_U + H_{\mathrm{bath}}$ of the Hamiltonian. The details of how the weights (21) are sampled and how the observables are measured depend on the specific continuous-time method.

3 Weak-coupling approach

The weak-coupling continuous-time impurity solver [6] expands the partition function in powers of $H_2{=}H_U$.[4] Equation (21) then gives the weight of a configuration of n *interaction vertices*. Since $H_1 = H - H_2 = H_\mu + H_{\mathrm{bath}} + H_{\mathrm{mix}}$ is quadratic, we can use Wick's theorem to evaluate the trace. The result is a product of two determinants of $n{\times}n$ matrices (one for each spin). The

[3] We can understand this formula by defining the operator $A(\beta) = e^{\beta H_1} e^{-\beta H}$ and writing the partition function as $Z = \mathrm{Tr}(e^{-\beta H_1} A(\beta))$. The operator $A(\beta)$ satisfies $dA/d\beta = e^{\beta H_1}(H_1 - H)e^{-\beta H} = -H_2(\beta)A(\beta)$, the solution of which is $A(\beta) = \mathcal{T}\exp\big(-\int_0^\beta d\tau H_2(\tau)\big)$.

[4] A related algorithm, based on an expansion in powers of $H_U - K/\beta$ (with K some non-zero constant), is the *continuous-time auxiliary field method* [7].

elements of these matrices are the Weiss Green functions $\mathcal{G}_0^\sigma$ for the time intervals defined by the vertex positions

$$\frac{w_C}{Z_0} = (-Ud\tau)^n \frac{1}{Z_0}\mathrm{Tr}\left(e^{-(\beta-\tau_n)H_1} n_\uparrow n_\downarrow \cdots e^{-(\tau_2-\tau_1)H_1} n_\uparrow n_\downarrow e^{-\tau_1 H_1}\right) = (-Ud\tau)^n \prod_\sigma \det M_\sigma^{-1},$$

where

$$\left(M_\sigma^{-1}\right)_{ij} = \mathcal{G}_0^\sigma(\tau_i - \tau_j) \quad \text{with} \quad \mathcal{G}_0^\sigma(\tau) = -\frac{1}{Z_0}\mathrm{Tr}\left(e^{-\beta H_1}\mathcal{T} d(\tau) d^\dagger(0)\right),$$

and $Z_0 = \mathrm{Tr}\, e^{-\beta H_1}$ is the partition function of the non-interacting model.[5] For the diagonal elements, we adopt the convention $(M_\sigma^{-1})_{ii} = \mathcal{G}_0^\sigma(0^-)$.

At this point, one notices a potential sign problem. In the paramagnetic phase, where $\mathcal{G}_0^\uparrow = \mathcal{G}_0^\downarrow$, the product of determinants is positive, which means that for a repulsive interaction ($U > 0$) odd perturbation orders yield negative weights. Except in the particle-hole symmetric case, where odd perturbation orders vanish, these odd order configurations cause a sign problem. Fortunately, we can solve this sign problem by shifting the chemical potentials for up and down spins in an appropriate way [6]. To do so, we rewrite the interaction term as [8]

$$H_U = \frac{U}{2}\sum_s \prod_\sigma \left(n_\sigma - \alpha_\sigma(s)\right) + \frac{U}{2}(n_\uparrow + n_\downarrow) + U\left(\left(\frac{1}{2}+\delta\right)^2 - \frac{1}{4}\right), \tag{22}$$

with

$$\alpha_\sigma(s) = \frac{1}{2} + \sigma s\left(\frac{1}{2}+\delta\right). \tag{23}$$

Here, δ is some constant and $s = \pm 1$ is an auxiliary Ising variable. This construction is not a Hubbard-Stratonovich transformation, but simply a shift in the zero of energy. The constant $U\left((\frac{1}{2}+\delta)^2 - \frac{1}{4}\right)$ in Eq. (22) is irrelevant and will be ignored in the following. We absorb the contribution $\frac{1}{2}U(n_\uparrow + n_\downarrow)$ into the non-interacting Green function by shifting the chemical potential as $\mu \to \mu - \frac{1}{2}U$. Explicitly, the Weiss Green function is redefined as[6]

$$\left(\mathcal{G}_0^\sigma\right)^{-1} = i\omega_n + \mu - \Delta^\sigma \;\to\; \left(\tilde{\mathcal{G}}_0^\sigma\right)^{-1} = i\omega_n + \mu - \tfrac{1}{2}U - \Delta^\sigma.$$

The introduction of an Ising variable s_i at each vertex position τ_i enlarges the configuration space exponentially. A configuration C now corresponds to a collection of auxiliary spin variables defined on the imaginary-time interval: $C = \{(\tau_1, s_1), (\tau_2, s_2), \ldots, (\tau_n, s_n)\}$. The weight of these configurations is

$$w_C = \tilde{Z}_0(-Ud\tau/2)^n \prod_\sigma \det \tilde{M}_\sigma^{-1}, \tag{24}$$

where

$$\left(\tilde{M}_\sigma^{-1}\right)_{ij} = \tilde{\mathcal{G}}_0^\sigma(\tau_i - \tau_j) - \alpha_\sigma(s_i)\delta_{ij}. \tag{25}$$

[5] We note that in the DMFT framework discussed in Section 1.2, the function $\mathcal{G}_0^\sigma$ is determined directly by the self-consistency loop, without reference to a Hamiltonian. For the purpose of the present discussion, we may however assume that we know H_{bath} and H_{mix} terms whose parameters yield $\mathcal{G}_0^\sigma$ through Eqs. (12) and (13).

[6] In a DMFT calculation, this means that the shifted chemical potential is used within the self-consistency loop.

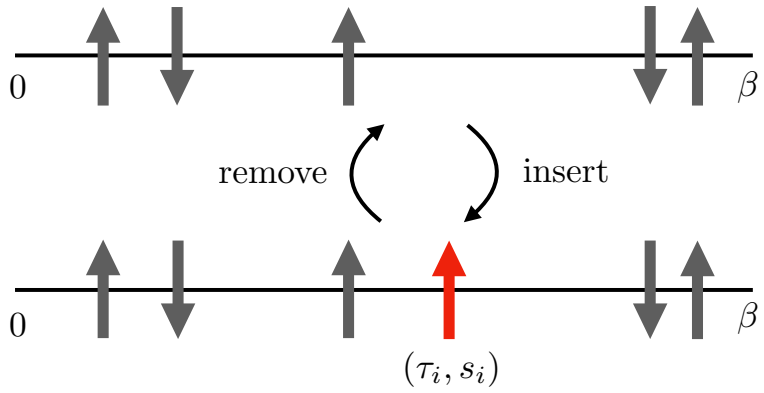

Fig. 2: *Local update in the weak-coupling method. The horizontal line represents the imaginary-time interval* $[0,\beta)$*. We increase the perturbation order by adding an auxiliary spin with random orientation at a random time and decrease it by removing a randomly chosen auxiliary spin.*

3.1 Sampling

For ergodicity it is sufficient that the sampling inserts the auxiliary spins with random orientation at random times and removes randomly chosen spins. Detailed balance requires that the probability $p(C\to C')$ to move from configuration C to C' satisfies $w(C)p(C\to C') = w(C')p(C'\to C)$. Splitting $p(C\to C') = p^{\text{prop}}(C\to C')p^{\text{acc}}(C\to C')$ into a proposal and acceptance probability, and using the Metropolis-Hastings algorithm [4], we have

$$p^{\text{acc}}(C\to C') = \min\big(1, \mathcal{R}(C\to C')\big),$$

where

$$\mathcal{R}(C\to C') = \frac{w(C')\,p^{\text{prop}}(C'\to C)}{w(C)\,p^{\text{prop}}(C\to C')}$$

and Eq. (24) is used to compute the ratio of the weights. To complete the description of the sampling we need to specify proposal probabilities for the insertion and removal of an auxiliary spin. A simple and reasonable procedure is illustrated in Fig. 2. For the insertion, we pick a random time in $[0,\beta)$ and a random orientation for the new spin, while for the removal, we simply pick a random spin. The corresponding proposal probabilities are

$$p^{\text{prop}}(n\to n{+}1) = \tfrac{1}{2}(d\tau/\beta), \quad p^{\text{prop}}(n{+}1\to n) = 1/(n{+}1). \tag{26}$$

The first step is choosing with equal probability whether we insert or remove. If we insert, then we are going from a configuration with n spins to a configuration with $n{+}1$ spins, and from Eq. (24) and the above choices for p^{prop}, the acceptance probability becomes $p^{\text{acc}}(n\to n{+}1) = \min\big(1, \mathcal{R}_{\text{insert}}(n\to n{+}1)\big)$ with

$$\mathcal{R}_{\text{insert}}(n\to n{+}1) = \frac{-\beta U}{n{+}1}\prod_\sigma \frac{\det\big(\tilde{M}_\sigma^{(n+1)}\big)^{-1}}{\det\big(\tilde{M}_\sigma^{(n)}\big)^{-1}}. \tag{27}$$

The acceptance probability for the removal follows from

$$\mathcal{R}_{\text{remove}}(n{+}1\to n) = 1/\mathcal{R}_{\text{insert}}(n\to n{+}1). \tag{28}$$

3.2 Determinant ratios and fast matrix updates

From Eq. (27), we see that each update requires the calculation of a ratio of two determinants. At first sight, one might think that for a matrix of size $n\times n$ this is an $\mathcal{O}(n^3)$ operation. However, each insertion or removal of a vertex (or spin) merely changes one row and one column of the matrix M_σ^{-1} (or $\tilde{M}_\sigma^{-1}$).[7] It is thus possible to evaluate this ratio in a time $\mathcal{O}(n^2)$ for insertion and $\mathcal{O}(1)$ for removal [3].

We first note that the objects which are stored and manipulated, besides the lists of the times $\{\tau_i\}$ (or times and spins $\{(\tau_i, s_i)\}$), are the matrices $M_\sigma = (\mathcal{G}_0^\sigma)^{-1}$, not $M_\sigma^{-1} = \mathcal{G}_0^\sigma$. Inserting a vertex (or auxiliary spin) adds a new row and column to M_σ^{-1}. We imagine inserting this row and column on the border of the given matrix and write the resulting matrix in a block matrix form (omitting the σ index for simplicity):

$$\left(M^{(n+1)}\right)^{-1} = \begin{pmatrix} \left(M^{(n)}\right)^{-1} & Q \\ R & S \end{pmatrix}.$$

The analogous blocks of the M matrix are defined as

$$M^{(n+1)} = \begin{pmatrix} \tilde{P} & \tilde{Q} \\ \tilde{R} & \tilde{S} \end{pmatrix}. \tag{29}$$

Here Q, R, and S are $n\times 1$, $1\times n$, and 1×1 matrices which contain the functions $\mathcal{G}_0$ evaluated at time intervals determined by the position of the new vertex (spin). They can be easily computed. We want to find $\tilde{P}$, $\tilde{Q}$, $\tilde{R}$, and $\tilde{S}$, and the ratio of determinants. Using the expression for the block inversion of a matrix and for the determinant of a block matrix, the determinant ratio needed for the acceptance probability becomes

$$\frac{\det\left(M^{(n+1)}\right)^{-1}}{\det\left(M^{(n)}\right)^{-1}} = \det\left(S - RM^{(n)}Q\right) = S - RM^{(n)}Q\,. \tag{30}$$

Because we store $M^{(n)}$, computing the acceptance probability of an insertion move is just an $\mathcal{O}(n^2)$ operation. If the move is accepted, the new matrix $M^{(n+1)}$ can be computed from $M^{(n)}$, Q, R, and S, also in a time $\mathcal{O}(n^2)$:

$$\tilde{S} = \left(S - (R)\,(M^{(n)}\,Q)\right)^{-1}, \tag{31}$$

$$\tilde{Q} = -(M^{(n)}Q)\,\tilde{S}, \tag{32}$$

$$\tilde{R} = -\tilde{S}\,(R\,M^{(n)}), \tag{33}$$

$$\tilde{P} = M^{(n)} + (M^{(n)}Q)\,\tilde{S}\,(RM^{(n)}). \tag{34}$$

In the case of removing a spin we imagine removing a bordering row and column. It follows from Eqs. (30) and (31) that

$$\frac{\det\left(M^{(n)}\right)^{-1}}{\det\left(M^{(n+1)}\right)^{-1}} = \det\tilde{S} = \tilde{S}. \tag{35}$$

[7] In the following, we write the formulas without the tildes, that is, for the sampling of interaction vertices. For the algorithm with auxiliary spins, it suffices to replace $M\to\tilde{M}$ and $\mathcal{G}_0\to\tilde{\mathcal{G}}_0$.

$\tilde{S}$ is just a 1×1 matrix so its determinant is trivial to compute. The above formulas also imply that the elements of the reduced matrix are

$$M^{(n)} \;=\; \tilde{P} - (\tilde{Q})(\tilde{R})/\tilde{S}. \tag{36}$$

The calculation of the removal probability is thus $\mathcal{O}(1)$, while the calculation of the new $M^{(n)}$ matrix is $\mathcal{O}(n^2)$.

3.3 Measurement of the Green function

To compute the contribution of a configuration C to the Green function, $G^\sigma_C(\tau)$, we insert in the right-hand side of Eq. (21) a creation operator $d^\dagger$ at time 0 and an annihilation operator d at time τ and divide by w_C. Wick's theorem and Eq. (30) then lead to the expression [6]

$$G^\sigma_C(\tau) \;=\; \mathcal{G}^\sigma_0(\tau) - \sum_k \mathcal{G}^\sigma_0(\tau-\tau_k) \sum_l \big(M_\sigma\big)_{kl}\, \mathcal{G}^\sigma_0(\tau_l). \tag{37}$$

The estimate for the impurity Green function for a given imaginary-time then follows from Eq. (19). To avoid unnecessary and time-consuming summations during the Monte Carlo simulation (evaluation of Eq. (37) for many τ-values), we accumulate the quantity [7]

$$S_\sigma(\tilde{\tau}) \equiv \sum_k \delta(\tilde{\tau}-\tau_k) \sum_l \big(M_\sigma\big)_{kl}\, \mathcal{G}^\sigma_0(\tau_l),$$

by binning the time points $\tilde{\tau}$ on a fine grid. After the simulation is finished, we compute the Green function as[8]

$$G^\sigma(\tau) = \mathcal{G}^\sigma_0(\tau) - \int_0^\beta d\tilde{\tau}\, \mathcal{G}^\sigma_0(\tau-\tilde{\tau}) \big\langle S_\sigma(\tilde{\tau}) \big\rangle_{\text{MC}}. \tag{38}$$

It is also possible to measure the Matsubara components of the Green function directly. Using the imaginary-time translational invariance of the Green functions, one finds

$$G^\sigma_C(i\omega_n) \;=\; \mathcal{G}^\sigma_0(i\omega_n) - \mathcal{G}^\sigma_0(i\omega_n) \sum_{kl} \frac{1}{\beta} e^{i\omega_n(\tau_k-\tau_l)} \big(M_\sigma\big)_{kl}\, \mathcal{G}^\sigma_0(i\omega_n),$$

so that

$$G^\sigma(i\omega_n) = \mathcal{G}^\sigma_0(i\omega_n) - \frac{1}{\beta}\big(\mathcal{G}^\sigma_0(i\omega_n)\big)^2 \left\langle \sum_{kl} e^{i\omega_n(\tau_k-\tau_l)} \big(M_\sigma\big)_{kl} \right\rangle_{\text{MC}}. \tag{39}$$

We note that because the Weiss Green function has the high-frequency behavior $\mathcal{G}_0(i\omega_n) \sim 1/i\omega_n$, the measured impurity Green function automatically inherits the correct high-frequency tail.

[8] Comparison of this equation with the Dyson equation $G = \mathcal{G}_0 + \mathcal{G}_0 \star \Sigma \star G$ (where the $\star$ symbol denotes a convolution in imaginary time) shows that his procedure amounts to measuring $-\Sigma \star G$.

3.4 Multi-orbital and cluster impurity problems

The generalization of the weak-coupling method to impurity clusters is straightforward. All we have to do is to add a site index to the interaction vertices (or auxiliary Ising spin variables) and sample the vertices (auxiliary spins) on a family of n_{sites} imaginary-time intervals.
General four-Fermion terms as in Eq. (2) are, at least in principle, also easily dealt with. We simply expand the partition function in powers of the interactions U^{abcd}. The trace over the impurity and bath degrees of freedom again yields a determinant of a matrix whose order equals the total perturbation order. In general there is a sign problem. To reduce the sign problem, it is advantageous to introduce auxiliary fields α and replace

$$\frac{1}{2}\sum_{abcd} U^{abcd}\, d_a^\dagger d_b^\dagger d_c d_d \rightarrow -\frac{1}{2}\sum_{abcd} U^{abcd}\big(d_a^\dagger d_c - \alpha_{ac}\big)\big(d_b^\dagger d_d - \alpha_{bd}\big),$$

with an appropriate shift in the quadratic part of the Hamiltonian. However, in general, it is not possible to completely eliminate the sign problem by a suitable choice of α parameters. Furthermore, since the number of interaction terms grows like $\mathcal{O}(n_{\text{orbitals}}^4)$, the computational cost rapidly escalates. In practice, the approach discussed in the following section is a more suitable approach for single-site multi-orbital impurity problems with general interactions.

4 Hybridization-expansion approach

While the Monte Carlo weights in the weak-coupling method are expressed in terms of the Weiss Green function $\mathcal{G}_0$, the hybridization-expansion method, which is in many ways complementary to the weak-coupling approach, naturally involves the hybridization function Δ. It follows from Eq. (13) that the Weiss Green function $\mathcal{G}_0$ and hybridization function Δ contain the same information, and the DMFT procedure sketched in Sec. 1.2 could be just as well written as a self-consistency loop fixing the hybridization function Δ.
The hybridization-expansion approach [9] is based on an expansion of the partition function in powers of the impurity-bath hybridization term. Here, we decompose the Hamiltonian as $H_2 = H_{\text{mix}}$ and $H_1 = H - H_2 = H_\mu + H_U + H_{\text{bath}}$. Since $H_2 \equiv H_2^{d^\dagger} + H_2^d = \sum_{p\sigma} V_{p\sigma}\, d_\sigma^\dagger c_{p\sigma} + \sum_{p\sigma} V_{p\sigma}^*\, c_{p\sigma}^\dagger d_\sigma$ has two terms, corresponding to electrons hopping from the bath to the impurity and from the impurity back to the bath, only even perturbation orders contribute to Eq. (20). Furthermore, at perturbation order $2n$, only the $(2n)!/(n!)^2$ terms corresponding to n creation operators $d^\dagger$ and n annihilation operators d contribute. We therefore write the partition function as a sum over configurations $\{\tau_1, \ldots, \tau_n; \tau_1', \ldots, \tau_n'\}$ that are collections of imaginary-time points corresponding to these n annihilation and n creation operators:

$$Z = \sum_{n=0}^{\infty} \int_0^\beta d\tau_1 \cdots \int_{\tau_{n-1}}^\beta d\tau_n \int_0^\beta d\tau_1' \cdots \int_{\tau_{n-1}'}^\beta d\tau_n' \,\text{Tr}\Big(e^{-\beta H_1}\mathcal{T} H_2^d(\tau_n) H_2^{d^\dagger}(\tau_n') \cdots H_2^d(\tau_1) H_2^{d^\dagger}(\tau_1')\Big). \tag{40}$$

Since the imaginary-time evolution operator $e^{-\tau H_1}$ does not rotate the spin in the case of the Anderson impurity model, the configurations must contain an equal number of creation and

annihilation operators for each spin. Taking this additional constraint into account and using the explicit expressions for H_2^d and $H_2^{d^\dagger}$, we find

$$\begin{aligned} Z &= Z_{\rm bath} \sum_{\{n_\sigma\}} \prod_\sigma \int_0^\beta d\tau_1^\sigma \cdots \int_{\tau_{n_\sigma-1}^\sigma}^\beta d\tau_{n_\sigma}^\sigma \int_0^\beta d\tau_1'^\sigma \ldots \int_{\tau_{n_\sigma-1}'^\sigma}^\beta d\tau_{n_\sigma}'^\sigma \\ &\quad \times {\rm Tr}_d \Big(e^{-\beta H_{\rm loc}} \mathcal{T} \prod_\sigma d_\sigma(\tau_{n_\sigma}^\sigma) d_\sigma^\dagger(\tau_{n_\sigma}'^\sigma) \ldots d_\sigma(\tau_1^\sigma) d_\sigma^\dagger(\tau_1'^\sigma) \Big) \\ &\quad \times \frac{1}{Z_{\rm bath}} {\rm Tr}_c \Big(e^{-\beta H_{\rm bath}} \mathcal{T} \prod_\sigma \sum_{p_1 \ldots p_{n_\sigma}} \sum_{p_1' \ldots p_{n_\sigma}'} V_{p_1\sigma}^* V_{p_1'\sigma} \cdots V_{p_{n_\sigma}\sigma}^* V_{p_{n_\sigma}'\sigma} \\ &\qquad c_{p_{n_\sigma}\sigma}^\dagger(\tau_{n_\sigma}^\sigma) c_{p_{n_\sigma}'\sigma}(\tau_{n_\sigma}'^\sigma) \ldots c_{p_1\sigma}^\dagger(\tau_1^\sigma) c_{p_1'\sigma}(\tau_1'^\sigma) \Big), \end{aligned}$$

where to separate the d and c operators we used the fact that H_1 does not mix the impurity and the bath. The local Hamiltonian $H_{\rm loc}$ is defined in Eq. (5) and $Z_{\rm bath} = {\rm Tr}_c\, e^{-\beta H_{\rm bath}}$.
Introducing the β-antiperiodic hybridization function (12), which in the time-domain reads

$$\Delta^\sigma(\tau) = \sum_p \frac{|V_{p\sigma}|^2}{e^{\varepsilon_p \beta} + 1} \begin{cases} -e^{-\varepsilon_p(\tau-\beta)} & 0 < \tau < \beta \\ e^{-\varepsilon_p \tau} & -\beta < \tau < 0 \end{cases},$$

the trace over the bath states can be expressed as

$$\begin{aligned} &\frac{1}{Z_{\rm bath}} {\rm Tr}_c \Big(e^{-\beta H_{\rm bath}} \mathcal{T} \prod_\sigma \sum_{p_1 \ldots p_{n_\sigma}} \sum_{p_1' \ldots p_{n_\sigma}'} V_{p_1\sigma}^* V_{p_1'\sigma} \cdots V_{p_{n_\sigma}\sigma}^* V_{p_{n_\sigma}'\sigma} \\ &\qquad c_{p_{n_\sigma}\sigma}^\dagger(\tau_{n_\sigma}^\sigma) c_{p_{n_\sigma}'\sigma}(\tau_{n_\sigma}'^\sigma) \cdots c_{p_1\sigma}^\dagger(\tau_1^\sigma) c_{p_1'\sigma}(\tau_1'^\sigma) \Big) = \prod_\sigma \det M_\sigma^{-1}, \end{aligned}$$

where M_σ^{-1} is the $(n_\sigma \times n_\sigma)$ matrix with elements

$$\big(M_\sigma^{-1}\big)_{ij} = \Delta^\sigma(\tau_i'^\sigma - \tau_j^\sigma).$$

In the hybridization expansion approach, the configuration space consists of all sequences $C = \{\tau_1^\uparrow, \ldots, \tau_{n_\uparrow}^\uparrow; \tau_1'^\uparrow, \ldots, \tau_{n_\uparrow}'^\uparrow | \tau_1^\downarrow, \ldots, \tau_{n_\downarrow}^\downarrow; \tau_1'^\downarrow, \ldots, \tau_{n_\downarrow}'^\downarrow\}$ of $n_\uparrow$ creation and annihilation operators for spin up ($n_\uparrow = 0, 1, \ldots$) and $n_\downarrow$ creation and annihilation operators for spin down ($n_\downarrow = 0, 1, \ldots$). The weight of such a configuration is

$$w_C = Z_{\rm bath} {\rm Tr}_d \Big(e^{-\beta H_{\rm loc}} \mathcal{T} \prod_\sigma d_\sigma(\tau_{n_\sigma}^\sigma) d_\sigma^\dagger(\tau_{n_\sigma}'^\sigma) \cdots d_\sigma(\tau_1^\sigma) d_\sigma^\dagger(\tau_1'^\sigma) \Big) \prod_\sigma \det M_\sigma^{-1} (d\tau)^{2n_\sigma}. \quad (41)$$

The trace factor represents the contribution of the impurity, which fluctuates between different quantum states as electrons hop in and out. The determinants sum up all bath evolutions which are compatible with the given sequence of transitions.
To evaluate the trace factor, we may for example use the eigenbasis of $H_{\rm loc}$. In this basis, the imaginary-time evolution operator $e^{-\tau H_{\rm loc}}$ is diagonal while the operators d_σ and $d_\sigma^\dagger$ produce transitions between eigenstates with amplitude ± 1. Because the time evolution does not flip the electron spin, the creation and annihilation operators for a given spin alternate. This observation

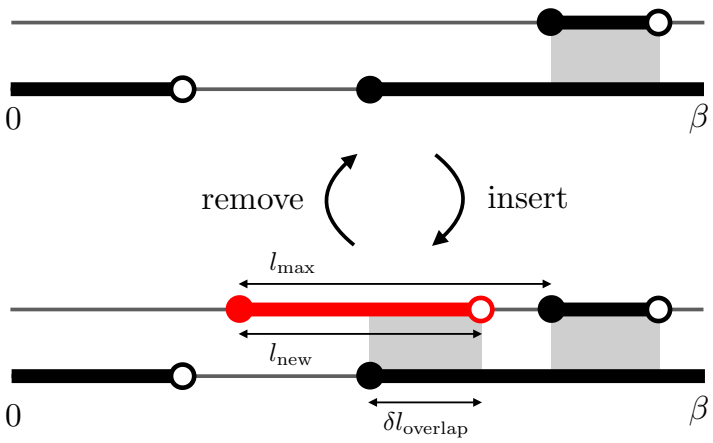

Fig. 3: *Local update in the segment picture. The two segment configurations correspond to spin up and down electrons. Each segment depicts a time interval in which an electron of the corresponding spin resides on the impurity. The segment end points are the locations of the operators $d^\dagger$ (full circles) and d (empty circles). We increase the perturbation order by adding a segment or anti-segment of random length for random spin and decrease it by removing a randomly chosen segment or anti-segment.*

allows us to separate the operators for spin up from those for spin down and to depict the time evolution by a *collection of segments* with each segment representing an imaginary-time interval in which an electron of spin up or down resides on the impurity (Fig. 3). We call an unoccupied time-interval between two segments an "anti-segment".
At each time, the eigenstate of the impurity follows immediately from the segment representation, and the trace factor becomes

$$\mathrm{Tr}_d\Big(e^{-\beta H_{\rm loc}}\mathcal{T}\prod_\sigma d_\sigma(\tau^\sigma_{n_\sigma})d^\dagger_\sigma(\tau'^\sigma_{n_\sigma})\cdots d_\sigma(\tau^\sigma_1)d^\dagger_\sigma(\tau'^\sigma_1)\Big) = \mathcal{S}\exp\Big(\mu(l_\uparrow+l_\downarrow) - U l_{\rm overlap}\Big), \quad (42)$$

with $\mathcal{S}$ being a permutation sign, l_σ the total "length" of the segments for spin σ, and $l_{\rm overlap}$ the total length of the overlap between spin-up and spin-down segments. The lower panel of Fig. 3 shows a configuration with two segments for spin up and one segment for spin down (note the periodic boundary conditions). The time intervals where segments overlap, indicated by gray rectangles, correspond to a doubly occupied impurity and cost a repulsion energy U.

4.1 Sampling

For ergodicity, it is sufficient to insert and remove pairs of creation and annihilation operators (segments or anti-segments) for spin up and down. One possible strategy for inserting a segment is the following: We select a random time in $[0,\beta)$ for the creation operator. If it falls on an existing segment, the impurity is already occupied and the move is rejected. If it falls on an empty space, we compute $l_{\rm max}$, the length from this selected time to the next segment (in the direction of increasing τ, taking into account the periodic boundary conditions).[9] Then we

[9] If there are no segments for the given spin, $l_{\rm max} = \beta$.

choose the position of the new annihilation operator randomly in this interval of length $l_{\max}$ (Fig. 3). If in the inverse procedure we propose to remove a randomly chosen segment for this spin, then the proposal probabilities for the insertion and removal are

$$p^{\text{prop}}(n_\sigma \to n_\sigma{+}1) = \frac{d\tau}{\beta}\frac{d\tau}{l_{\max}}, \quad p^{\text{prop}}(n_\sigma{+}1 \to n_\sigma) = \frac{1}{n_\sigma + 1}.$$

The acceptance probability for the insertion of a segment becomes $p^{\text{acc}}(n_\sigma \to n_\sigma{+}1) = \min\bigl(1, \mathcal{R}_{\text{insert}}(n_\sigma \to n_\sigma{+}1)\bigr)$, with

$$\mathcal{R}_{\text{insert}}(n_\sigma \to n_\sigma{+}1) = \frac{\beta l_{\max}}{n_\sigma + 1}\, e^{\mu l_{\text{new}} - U\delta l_{\text{overlap}}} \frac{\det\left(M_\sigma^{(n_\sigma+1)}\right)^{-1}}{\det\left(M_\sigma^{(n_\sigma)}\right)^{-1}}, \tag{43}$$

while the acceptance probability for a removal is obtained from

$$\mathcal{R}_{\text{remove}}(n_\sigma{+}1 \to n_\sigma) = 1/\mathcal{R}_{\text{insert}}(n_\sigma \to n_\sigma{+}1). \tag{44}$$

Here, l_{new} is the length of the new segment, and $\delta l_{\text{overlap}}$ is the change in the overlap (see Fig. 3). We compute the ratio of determinants using the fast update formulas discussed in Section 3.2.

4.2 Measurement of the Green function

The strategy is to create configurations which contribute to the Green function measurement by decoupling the bath from a given pair of creation and annihilation operators in C. We start by expressing the expectation value for the Green function as

$$G(\tau) = -\frac{1}{Z}\sum_C w_C^{d(\tau)d^\dagger(0)} = -\frac{1}{Z}\sum_C w_C^{(\tau,0)}\, \frac{w_C^{d(\tau)d^\dagger(0)}}{w_C^{(\tau,0)}},$$

where $w_C^{d(\tau)d^\dagger(0)}$ denotes the weight of the configuration C with an additional operator $d^\dagger(0)$ and $d(\tau)$ in the trace factor and $w_C^{(\tau,0)}$ denotes the complete weight corresponding to the enlarged operator sequence (including enlarged hybridization determinants). Since the trace factors of both weights are identical, up to a permutation sign $(-1)^{i+j}$,

$$\frac{w_C^{d(\tau)d^\dagger(0)}}{w_C^{(\tau,0)}} = \frac{(-1)^{i+j}\det\left(M_C\right)^{-1}}{\det\left(M_C^{(\tau,0)}\right)^{-1}} = \left(M_C^{(\tau,0)}\right)_{ji},$$

with i and j denoting the row and column corresponding to the additional operators $d^\dagger$ and d in the enlarged $\big(M_C^{(\tau,0)}\big)^{-1}$. Hence, the measurement formula for the Green function becomes[10]

$$G(\tau) = -\frac{1}{Z}\sum_C w_C^{(\tau,0)}\big(M_C^{(\tau,0)}\big)_{ji} = -\frac{1}{Z}\sum_{\tilde{C}} w_{\tilde{C}}\tilde{n}^2\delta(\tau_{\tilde{n}}-\tau)\delta(\tau'_{\tilde{n}}-0)\big(M_{\tilde{C}}\big)_{\tilde{n}\tilde{n}}$$
$$= -\frac{1}{Z}\sum_{\tilde{C}} w_{\tilde{C}}\tilde{n}^2\frac{1}{\beta}\delta(\tau,\tau_{\tilde{n}}-\tau'_{\tilde{n}})\big(M_{\tilde{C}}\big)_{\tilde{n}\tilde{n}},$$

with $\delta(\tau,\tau') = \delta(\tau-\tau')$ for $\tau' > 0$, and $\delta(\tau,\tau') = -\delta(\tau-\tau'-\beta)$ for $\tau' < 0$. In the first step, we went from a sum over configurations C with n creation and annihilation operators in addition to $d(\tau)$ and $d^\dagger(0)$ to a sum over configurations $\tilde{C}$ with $\tilde{n} = n+1$ operator pairs, while in the last step, we used the translational invariance and the β-anti-periodicity of the Green function. We finally replace the factor $\tilde{n}^2$ (which comes from the $1/(n!)^2$ factor in the Monte Carlo weights without time ordering) by a sum over all pairs i,j of creation and annihilation operators, to obtain the measurement formula $G(\tau) = -\frac{1}{Z}\sum_{\tilde{C}} w_{\tilde{C}}\sum_{ij}\frac{1}{\beta}\delta(\tau,\tau_j-\tau'_i)\big(M_{\tilde{C}}\big)_{ji}$, or

$$G(\tau) = \left\langle -\sum_{ij}\frac{1}{\beta}\delta(\tau,\tau_i-\tau'_j)M_{ij}\right\rangle_{\text{MC}}. \tag{45}$$

Fourier transformation of Eq. (45) yields the measurement formula

$$G(i\omega_n) = \left\langle -\sum_{ij}\frac{1}{\beta}e^{i\omega_n(\tau_i-\tau'_j)}M_{ij}\right\rangle_{\text{MC}} \tag{46}$$

for the Fourier coefficients of the Green function. Note that in contrast to the weak-coupling approach, where we measure the Green function as a $\mathcal{O}(1/(i\omega_n)^2)$ correction to the Weiss Green function, Eq. (46) does not automatically yield the correct high frequency tail.

An elegant way to suppress the noise in $G(i\omega_n)$ at large ω_n and to obtain a compact representation of the Green function is to measure the expansion coefficients in a basis of orthogonal

[10] For the purpose of this derivation, it is convenient to use configurations C and $\tilde{C}$ without time ordering, that is, we write the Green function as

$$\begin{aligned}
G(\tau) =& -\frac{Z_{\text{bath}}}{Z}\sum_n\frac{1}{n!^2}\int_0^\beta d\tau_1\cdots d\tau_n\int_0^\beta d\tau'_1\cdots d\tau'_n\\
&\times \mathrm{Tr}_d\Big(e^{-\beta H_{\text{loc}}}\mathcal{T}d(\tau)d^\dagger(0)d(\tau_n)d^\dagger(\tau'_n)\cdots d(\tau_1)d^\dagger(\tau'_1)\Big)\det\big(M^{(\tau,0)}\big)^{-1}\big(M^{(\tau,0)}\big)_{n+1,n+1}\\
=& -\frac{Z_{\text{bath}}}{Z}\sum_n\frac{(n+1)^2}{\big((n+1)!\big)^2}\int_0^\beta d\tau_1\cdots d\tau_{n+1}\int_0^\beta d\tau'_1\cdots d\tau'_{n+1}\delta(\tau_{n+1}-\tau)\delta(\tau'_{n+1}-0)\\
&\times \mathrm{Tr}_d\Big(e^{-\beta H_{\text{loc}}}\mathcal{T}d(\tau_{n+1})d^\dagger(\tau'_{n+1})d(\tau_n)d^\dagger(\tau'_n)d(\tau_1)d^\dagger(\tau'_1)\Big)\det\big(M^{(\tau,0)}\big)^{-1}\big(M^{(\tau,0)}\big)_{n+1,n+1}\\
=& -\frac{Z_{\text{bath}}}{Z}\sum_{\tilde{n}}\frac{\tilde{n}^2}{(\tilde{n}!)^2}\int_0^\beta d\tau_1\cdots d\tau_{\tilde{n}}\int_0^\beta d\tau'_1\cdots d\tau'_{\tilde{n}}\delta(\tau_{\tilde{n}}-\tau)\delta(\tau'_{\tilde{n}}-0)\\
&\times \mathrm{Tr}_d\Big(e^{-\beta H_{\text{loc}}}\mathcal{T}d(\tau_{\tilde{n}})d^\dagger(\tau'_{\tilde{n}})\cdots d(\tau_1)d^\dagger(\tau'_1)\Big)\det\big(M^{(\tilde{n})}\big)^{-1}\big(M^{(\tilde{n})}\big)_{\tilde{n}\tilde{n}}.
\end{aligned}$$

polynomials [10]. A suitable choice are the *Legendre polynomials* $P_l(x)$ defined on $x \in [-1,1]$ through the recursion relation

$$\begin{aligned} P_0(x) &= 1, \\ P_1(x) &= x, \\ (l{+}1)P_{l+1}(x) &= (2l{+}1)xP_l(x) - lP_{l-1}(x). \end{aligned}$$

The P_l furthermore satisfy $\int_{-1}^{1} dx\, P_k(x)P_l(x) = \frac{2}{2l+1}\delta_{kl}$. Defining $x(\tau) = 2\tau/\beta{-}1$, one can thus express the Green function on the interval $\tau \in [0,\beta]$ as

$$G(\tau) = \sum_{l\geq 0} \frac{\sqrt{2l+1}}{\beta} P_l\big(x(\tau)\big) G_l, \tag{47}$$

$$G_l = \sqrt{2l+1} \int_0^\beta d\tau P_l\big(x(\tau)\big) G(\tau). \tag{48}$$

The advantage of the Legendre representation over the Matsubara representation is a much faster decay of the expansion coefficients with increasing order. The Matsubara Fourier transform requires anti-periodization of the Green function with discontinuities at $\tau = m\beta$, which leads to slowly decaying Matsubara coefficients ($G(i\omega_n) \sim 1/i\omega_n$ for large ω_n). On the other hand, the Legendre basis represents the smooth function $G(\tau)$ on the interval $[0,\beta]$. In practice, 30 to 50 Legendre coefficients are enough to reproduce the Green function with high precision and neglecting the higher orders acts as a convenient noise filter.
From Eqs. (45) and (48) it follows that

$$G_l = \left\langle -\sum_{ij} \frac{\sqrt{2l+1}}{\beta} \tilde{P}_l(\tau_i{-}\tau'_j) M_{ij} \right\rangle_{\text{MC}}, \tag{49}$$

with $\tilde{P}_l(\tau) = P_l\big(x(\tau)\big)$ for $\tau > 0$ and $\tilde{P}_l(\tau) = -P_l\big(x(\tau{+}\beta)\big)$ for $\tau < 0$.
The Matsubara coefficients are obtained from the Legendre coefficients as $G(i\omega_n) = \sum_{l\geq 0} T_{nl} G_l$, with the unitary transformation T_{nl} given by $T_{nl} = (-1)^n i^{l+1}\sqrt{2l+1}\, j_l(\frac{1}{2}\beta\omega_n)$, which involves the spherical Bessel functions $j_l(z)$. In the limit $n \to \infty$, T_{nl} decays $\sim 1/(i\omega_n)$ for n even and $\sim 1/(i\omega_n)^2$ for n odd.
An even more compact representation of Green functions can be obtained with the so-called intermediate representation introduced in Ref. [11].

4.3 Generalizations – Matrix and Krylov formalisms

4.3.1 Matrix formalism

It is obvious from the above derivation that the hybridization-expansion formalism is applicable to general classes of impurity models [12]. Because we compute the trace factor in the weight (41) exactly, H_{loc} can contain arbitrary local interactions (for example, spin-exchange terms in multi-orbital models), degrees of freedom (for example, spins in Kondo-lattice models) or constraints (for example, 'no double occupancy' in the t-J model).

For multi-orbital impurity models with $H_{\rm loc}$ diagonal in the occupation number basis, such as models with density-density interactions, the segment formalism illustrated in Fig. 3 is still applicable, but there is now a collection of segments for each *flavor* α (orbital, spin, etc.). The trace factor can again be computed from the length of the segments (the chemical potential contribution) and the overlaps between segments of different flavor (the interaction contribution). This allows a very efficient simulation of models with 5, 7, and in principle even more orbitals, despite the fact that the corresponding Hilbert spaces ($4^5 = 1024$ for 5 orbitals, $4^7 = 16384$ for 7 orbitals) are quite large.

If $H_{\rm loc}$ is not diagonal in the occupation number basis defined by the $d^\dagger_\alpha$, the calculation of

$$\mathrm{Tr}_d\Big(e^{-\beta H_{\rm loc}}\mathcal{T}\prod_\alpha d_\alpha(\tau^\alpha_{n_\alpha})\,d^\dagger_\alpha(\tau'^\alpha_{n_\alpha})\cdots d_\sigma(\tau^\alpha_1)\,d^\dagger_\alpha(\tau'^\alpha_1)\Big) \tag{50}$$

becomes rather involved and for a model with a large Hilbert space also computationally expensive. An obvious idea is to evaluate the trace in the eigenbasis where the imaginary-time evolution operators $e^{-H_{\rm loc}\tau}$ become diagonal. On the other hand, the operators d_α and $d^\dagger_\alpha$, which are simple and sparse in the occupation number basis, become complicated matrices in the eigenbasis. The evaluation of the trace factor in the eigenbasis thus involves the multiplication of matrices whose size scales as the dimension of the Hilbert space of the local problem. Since the dimension of this Hilbert space grows *exponentially* with the number of flavors, the calculation of the trace factor becomes the computational bottleneck of the simulation, and the matrix formalism is therefore restricted to a relatively small number of flavors.

It is important to identify and use *conserved quantum numbers* [13]. Typically, these are particle number for spin up and spin down and momentum. If we group the eigenstates of $H_{\rm loc}$ according to these quantum numbers, the operator matrices acquire a sparse block structure. For example, the operator $d^\dagger_{\uparrow,q}$ connects states corresponding to the quantum numbers $m = \{n_\uparrow, n_\downarrow, k, \ldots\}$ to those with $m' = \{n_\uparrow{+}1, n_\downarrow, k{+}q, \ldots\}$ (if they exist). Checking the compatibility of the operator sequence with the different starting blocks allows us to identify the blocks which contribute to the trace without performing any expensive matrix-matrix multiplications.

Let us take as a simple example a two-orbital model with conserved quantum numbers $n_\uparrow$ and $n_\downarrow$. The operator sequence $d^\dagger_\uparrow(\tau_4)\,d^\dagger_\uparrow(\tau_3)\,d_\uparrow(\tau_2)\,d_\uparrow(\tau_1)$ (with $\tau_1 < \tau_2 < \tau_3 < \tau_4$) is compatible with the starting blocks $\{n_\uparrow = 2; n_\downarrow = 0, 1, 2\}$, since the quantum numbers evolve as

$$\{n_\uparrow = 2; n_\downarrow\} \underset{d_\uparrow}{\to} \{n_\uparrow = 1; n_\downarrow\} \underset{d_\uparrow}{\to} \{n_\uparrow = 0; n_\downarrow\} \underset{d^\dagger_\uparrow}{\to} \{n_\uparrow = 1; n_\downarrow\} \underset{d^\dagger_\uparrow}{\to} \{n_\uparrow = 2; n_\downarrow\},$$

whereas the blocks $\{n_\uparrow = 0, 1; n_\downarrow = 0, 1, 2\}$ do not contribute to the weight, since, for example,

$$\{n_\uparrow = 1; n_\downarrow\} \underset{d_\uparrow}{\to} \{n_\uparrow = 0; n_\downarrow\} \underset{d_\uparrow}{\to} \emptyset\,.$$

Having identified the contributing blocks, the trace calculation reduces to a block matrix multiplication of the form

$$\sum_{\substack{\text{contributing}\\ m}} \mathrm{Tr}_m\Big(\cdots\big(O\big)_{m''m'}\big(e^{-(\tau'-\tau)H_{\rm loc}}\big)_{m'}\big(O\big)_{m'm}\big(e^{-\tau H_{\rm loc}}\big)_m\Big), \tag{51}$$

where O is either a creation or annihilation operator, m denotes the index of the matrix block, and the sum runs over those starting sectors which are compatible with the operator sequence. Using the block structure imposed by the conserved quantum numbers, it is possible to efficiently simulate 3-orbital models or 4-site clusters. However, since the matrix blocks are dense and the largest blocks grow exponentially with system size, the simulation of 5-orbital models already becomes quite expensive and the simulation of 7-orbital models with 5, 6 or 7 electrons is doable only if we truncate the size of the blocks.
In fact, one should distinguish two types of truncations:

1. Restriction of the trace $\sum_{\text{contributing } m} \mathrm{Tr}_m(\ldots)$ to those quantum number sectors or states which give the dominant contribution,

2. Reduction of the size of the operator blocks $\big(O\big)_{m'm''}$ by eliminating high-energy states.

Truncations of type (1) have little effect at low enough temperature, because they restrict the possible states only at a single point on the imaginary-time interval. Truncations of the type (2) are more problematic and possibly lead to systematic errors which are difficult to estimate and control when the system size is large.
Accumulating a histogram of the states or quantum number sectors visited during the sampling can be very instructive. For example, in the study of correlated materials with multiple partially filled orbitals, interesting questions are the typical valence or the dominant spin state, and the importance of fluctuations to other charge and spin states. Dynamical mean-field theory allows us to address these issues by adopting a real-space representation of the solid as a collection of atoms and treating the local fluctuations on a given site through the effective impurity model construction. The strong-coupling solver, which treats the local part of the impurity problem exactly, is ideally suited for such an analysis.

4.3.2 Krylov formalism

An alternative strategy [14] to evaluate the trace factor (50) is to

1. Adopt the occupation number basis in which we can easily apply the d_α and $d_\alpha^\dagger$ operator matrices to any state and in which we can exploit the sparse nature of H_{loc} during the imaginary-time evolutions,

2. Approximate the trace by a sum over the lowest energy states, that is, by a truncation of type (1) described in the previous subsection.

Instead of evaluating the matrix corresponding to the product of operators, we propagate each retained state in the trace through the sequence of time-evolution, creation and annihilation operators. This computation only involves matrix-vector multiplications of the type $d_\alpha|v\rangle$, $d_\alpha^\dagger|v\rangle$, and $H_{\text{loc}}|v\rangle$ with *sparse* operators d_α, $d_\alpha^\dagger$ and H_{loc} and is thus possible for systems for which the multiplication of dense matrix blocks becomes prohibitively expensive. Furthermore, the approach does not require any approximation of type (2), so all excited states remain accessible at intermediate τ. While the sparsity of H_{loc} depends on the number of interaction terms,

this number grows at most proportionally to the number of orbitals squared. In contrast, the dimension of the matrix grows exponentially with the number of orbitals.
The expensive step is the calculation of the time evolution from one operator to the next. We evaluate the matrix exponentials applied to a vector, $\exp(-\tau H_{\text{loc}})|v\rangle$, by iteratively constructing the *Krylov space*

$$\mathcal{K}_p(|v\rangle) = \text{span}\{|v\rangle, H_{\text{loc}}|v\rangle, H_{\text{loc}}^2|v\rangle, \ldots, H_{\text{loc}}^p|v\rangle\}$$

and by approximating the full matrix exponential by the matrix exponential of the Hamiltonian projected onto $\mathcal{K}_p(|v\rangle)$. The iteration number p is determined by tracking the convergence of $\exp(-\tau H_{\text{loc}})|v\rangle$ and stopping the calculation if the difference between iteration p and $p+1$ drops below some cutoff value. The number of iterations depends on the time interval τ, but typically, convergence occurs for very small iteration numbers $p \ll N_{\text{dim}}$, with N_{dim} the dimension of the Hilbert space.
In the limit where the dimension of the local Hilbert space N_{dim} is large, the Krylov approach is more efficient than an implementation based on a matrix representation of the operators d_α, $d_\alpha^\dagger$ and an evaluation of the trace of the matrix product. If the Monte Carlo configuration has n creation and n annihilation operators and we perform the trace over $N_{\text{tr}} \leq N_{\text{dim}}$ states, the Krylov calculation of the trace scales as

$$\mathcal{O}\big(N_{\text{tr}} N_{\text{dim}} 2n(1+\langle p\rangle)\big),$$

where the first term comes from the application of the creation and annihilation operators and the second term, proportional to the average dimension $\langle p\rangle$ of the Krylov space, from the application of the time-evolution operators. If we retain all the states in the trace calculation, $N_{\text{tr}} = N_{\text{dim}}$, and the trace calculation scales as N_{dim}^2. If we restrict the trace to a small number of low-energy states, then N_{tr} is $\mathcal{O}(1)$ and the trace computation becomes *linear* in N_{dim}. This scaling should be compared with a computational effort of $\mathcal{O}(2nN_{\text{dim}}^3)$ for the evaluation of the trace based on matrix multiplications (without truncation of the matrix blocks).[11]
While in theory the Krylov space approach is the method of choice due to its superior N_{dim} scaling, in practice the precise numbers of N_{tr}, $\langle p\rangle$, and N_{dim} determine which one of the two approaches performs better for a given problem. Experience shows that for five orbital problems the Krylov approach becomes superior to the matrix method.

5 Scaling of the algorithms

In the weak-coupling and hybridization-expansion algorithms, the average expansion orders have a simple physical interpretation: In a DMFT calculation, they yield highly accurate measurements for the potential and kinetic energy.
Let us first consider the weak-coupling algorithm, where after the introduction of auxiliary fields (Eqs. (22) and (23)) and the shifting of the chemical potential one obtains $H = H_1 + H_2$, with

[11] In the truncated trace approach, it is important to measure the various local observables at $\tau = \frac{1}{2}\beta$ where they are least affected by the truncation at $\tau = 0$ and $\tau = \beta$. Also, it is important not to destroy the multiplet structure when truncating the trace.

$H_1 = H_\mu + \frac{1}{2}U(n_\uparrow{+}n_\downarrow) + H_{\text{bath}}$ and $H_2 = Un_\uparrow n_\downarrow - \frac{1}{2}U(n_\uparrow{+}n_\downarrow)$.[12] It follows from Eq. (20) that

$$\begin{aligned}\langle -H_2\rangle &= \frac{1}{\beta}\int_0^\beta d\tau \left\langle -H_2(\tau)\right\rangle \\ &= \frac{1}{\beta}\frac{1}{Z}\sum_{n=0}^{\infty}\frac{n{+}1}{(n{+}1)!}\int_0^\beta d\tau\int_0^\beta d\tau_1\cdots\int_0^\beta d\tau_n \mathrm{Tr}\Big(e^{-\beta H_1}\mathcal{T}(-H_2(\tau))(-H_2(\tau_n))\cdots(-H_2(\tau_1))\Big) \\ &= \frac{1}{\beta}\frac{1}{Z}\sum_C n_C w_C = \frac{1}{\beta}\langle n\rangle, \end{aligned} \tag{52}$$

and therefore the average perturbation order $\langle n\rangle$ is related to the potential energy by

$$\langle n\rangle_{\text{weak-coupling}} = -\beta U\langle n_\uparrow n_\downarrow\rangle + \tfrac{1}{2}\beta U\langle n_\uparrow{+}n_\downarrow\rangle = -\beta E_{\text{pot}} + \tfrac{1}{2}\beta U\langle n_\uparrow{+}n_\downarrow\rangle. \tag{53}$$

We learn from this formula that the average perturbation order is roughly proportional to the inverse temperature β and the interaction strength U.

In the hybridization-expansion case, the average perturbation order is proportional to the kinetic energy. In single-site DMFT, we can express the kinetic energy

$$E_{\text{kin}} = \sum_{k\sigma}\epsilon_k G_{k\sigma}(0^-)$$

in terms of the Green function and hybridization function:[13]

$$E_{\text{kin}} = \sum_\sigma\int_0^\beta d\tau\, G_\sigma(\tau)\Delta^\sigma(-\tau).$$

[12] For simplicity, we have chosen $\delta = 0$.

[13] The first step in the derivation of this formula is to switch to the Fourier representation:

$$E_{\text{kin}} = \sum_{k\sigma}\epsilon_k G_{k\sigma}(0^-) = \sum_{k\sigma}\epsilon_k\frac{1}{\beta}\sum_n e^{-i\omega_n 0^-}G_{k\sigma}(i\omega_n) = \sum_{k\sigma}\epsilon_k\frac{1}{\beta}\sum_n e^{i\omega_n 0^+}\frac{1}{i\omega_n{+}\mu{-}\epsilon_k - \Sigma_\sigma(i\omega_n)}.$$

Introducing the density of states $\mathcal{D}(\epsilon)$, we can then write

$$\begin{aligned}E_{\text{kin}} &= \sum_\sigma\frac{1}{\beta}\sum_n e^{i\omega_n 0^+}\int d\epsilon\,\frac{\epsilon}{i\omega_n{+}\mu{-}\epsilon - \Sigma_\sigma(i\omega_n)}\,\mathcal{D}(\epsilon) \\ &= \sum_\sigma\frac{1}{\beta}\sum_n e^{i\omega_n 0^+}\int d\epsilon\,\frac{-\big(i\omega_n{+}\mu{-}\epsilon - \Sigma_\sigma(i\omega_n)\big) + \big(i\omega_n{+}\mu{-}\Sigma_\sigma(i\omega_n)\big)}{i\omega_n{+}\mu{-}\epsilon - \Sigma_\sigma(i\omega_n)}\,\mathcal{D}(\epsilon) \\ &= \sum_\sigma\frac{1}{\beta}\sum_n e^{i\omega_n 0^+}\Big(-1 + \big(i\omega_n{+}\mu - \Sigma_\sigma(i\omega_n)\big)G^\sigma_{\text{loc}}(i\omega_n)\Big),\end{aligned}$$

with G_{loc} the local lattice Green function, which after convergence of the DMFT calculation is identical to the impurity Green function G. The latter is related to the hybridization function by $G = (i\omega_n{+}\mu - \Sigma - \Delta)^{-1}$. Hence, we obtain

$$E_{\text{kin}} = \sum_\sigma\frac{1}{\beta}\sum_n e^{i\omega_n 0^+}G_\sigma(i\omega_n)\Delta^\sigma(i\omega_n) = \sum_\sigma\int d\tau\, G_\sigma(\tau)\Delta^\sigma(-\tau).$$

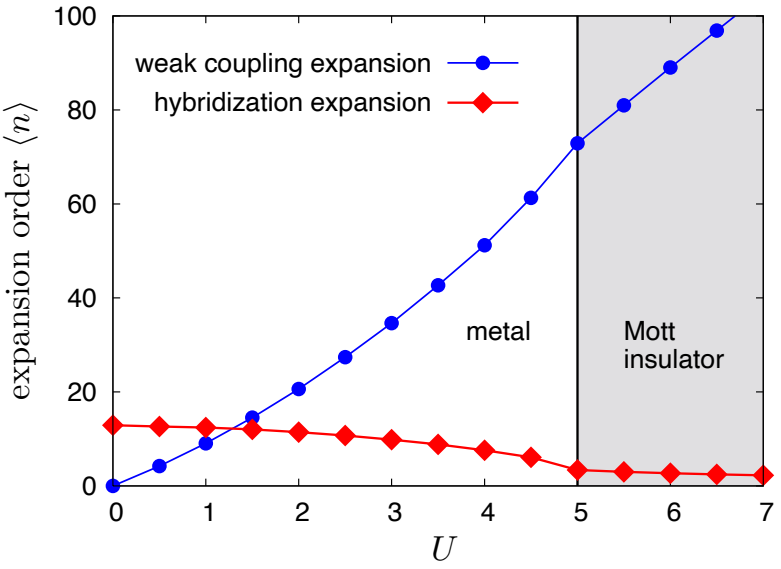

Fig. 4: *Average perturbation order for the weak-coupling and hybridization-expansion algorithms. These results correspond to the DMFT solution of the one-band Hubbard model with semi-circular density of states of bandwidth* 4 *and temperature* $T = 1/30$ *[15]. The bath is therefore different for each data point.*

Substituting the strong-coupling measurement formula (45) for G into this expression, one finds

$$E_{\rm kin} = \sum_\sigma \int_0^\beta d\tau \Big\langle -\sum_{ij} \frac{1}{\beta}\, \delta(\tau, \tau_i - \tau'_j)\, \big(M_\sigma\big)_{ij} \Big\rangle_{\rm MC} \Delta^\sigma(-\tau)$$
$$= -\sum_\sigma \Big\langle \frac{1}{\beta} \sum_{ij} \big(M_\sigma\big)_{ij}\, \Delta^\sigma(\tau'_j - \tau_i) \Big\rangle_{\rm MC} .$$

Now we use that $\big(M_\sigma\big)_{ij} = (-1)^{i+j} \det M_\sigma^{-1}[j,i] / \det M_\sigma^{-1}$, where $M_\sigma^{-1}[j,i]$ denotes the hybridization matrix with row j and column i removed. Hence, the sum

$$\sum_j (-1)^{i+j} \det M_\sigma^{-1}[j,i] \Delta^\sigma(\tau'_j - \tau_i) = \det M_\sigma^{-1}$$

appearing in the numerator is nothing but the expansion of the determinant of the hybridization matrix along column i. The expression for the kinetic energy thus simplifies to

$$E_{\rm kin} = -\sum_\sigma \Big\langle \frac{1}{\beta} \sum_i \frac{\det M_\sigma^{-1}}{\det M_\sigma^{-1}} \Big\rangle_{\rm MC} = -\frac{1}{\beta} \sum_\sigma \langle n_\sigma \rangle \,, \tag{54}$$

and the average total perturbation order $\langle n \rangle$ of the Monte Carlo configuration is related to the kinetic energy by

$$\langle n \rangle_{\text{hybridization-expansion}} = -\beta E_{\rm kin}.$$

While the average expansion order in both the weak-coupling and hybridization-expansion methods scales as β, the scaling of the expansion order with the interaction strength is very different. In the weak-coupling approach it grows roughly proportional to U, while in the

Solver	Scaling		Use
Weak-coupling	β^3	L^3	Impurity clusters with density-density interaction
Hybridization expansion (segment formalism)	β^3	L	Single-site multi-orbital models with density-density interaction
Hybridization expansion (matrix/Krylov formalism)	β	e^L	Single-site multi-orbital models with general U_{ijkl}

Table 1: *Scaling of the different impurity solvers with inverse temperature β and system size L. In the case of the segment algorithm, we assume that the calculation of the determinant ratios dominates the overlap calculations. In the matrix or Krylov case, we assume that the trace calculation dominates the calculation of the determinant ratios.*

hybridization-expansion approach, it decreases with increasing U (Fig. 4). In the case of the Anderson impurity model, this behavior leads to a significant computational speed-up for the hybridization-expansion approach in the intermediate- and large-U regime. Since local updates are $\mathcal{O}(n^2)$, a full sweep (update of all vertices in a configuration) is order $\mathcal{O}(n^3)$.
For impurity clusters, or models with complicated interaction terms, which require the matrix or Krylov formalisms discussed in Section 4.3, the hybridization-expansion method scales exponentially with system size, and we can only apply it to relatively small systems. Here, the weak-coupling approach, if applicable, can be the method of choice. Table 1 gives a summary of the different scalings (assuming a diagonal hybridization) and indicates which solver is appropriate for which type of problem. The weak-coupling solvers are mainly used in cluster DMFT calculations of the Hubbard model, where the polynomial scaling allows to treat clusters of up to 100 sites [16], at least in parameter regimes where there is no serious sign problem. The strong-coupling approach, on the other hand, is useful in particular for the study of (single-site) multi-orbital problems with complicated local interactions. Such problems typically have to be solved in single-site DMFT studies of strongly correlated materials, or in realistic simulations of transition metal impurities [17].

6 Electron-boson systems

6.1 Local phonons

In this section, we consider a quantum impurity model in which dispersionless phonons of frequency ω_0 couple to the electron density on the impurity site. The local term of the Anderson-Holstein impurity Hamiltonian $H = H_{\text{loc}} + H_{\text{mix}} + H_{\text{bath}}$ is

$$H_{\text{loc}} = -\mu(n_\uparrow + n_\downarrow) + U n_\uparrow n_\downarrow + g\big(n_\uparrow + n_\downarrow - 1\big)\big(b^\dagger + b\big) + \omega_0\, b^\dagger b. \tag{55}$$

Here, b and $b^\dagger$ denote the phonon annihilation and creation operators. An impurity model of this type has to be solved in single-site DMFT simulations of the Holstein-Hubbard model.

The bosonic sector of the Hilbert space of $H_{\rm loc}$ contains an infinite number of states. Hamiltonian-based impurity solvers truncate the Hilbert space to a finite number of phonon states, but treating even a truncated space may be computationally expensive. An attractive feature of the action-based continuous-time Monte Carlo formalism is that the phonons are integrated out, which both in the weak-coupling and the hybridization-expansion algorithms allows to treat the bosonic contribution in an elegant and efficient way.

We only discuss here the hybridization-expansion approach [18] which is based on a canonical transformation [19] called the *Lang-Firsov transformation*. This transformation decouples the electrons and phonons in the local Hamiltonian and applies to the physically relevant situation where the phonons couple to the total charge on the impurity atom. In this particular case, the electron-phonon coupling can be treated at essentially no additional computation cost.

At expansion order n_σ for spin σ, the $n_\sigma!$ diagrams corresponding to a given time sequence of fermionic creation and annihilation operators can be summed up into a determinant of a matrix M_σ^{-1}, as discussed in Sec. 4, so that the weight of the Monte Carlo configuration can be expressed as

$$w(\{O_i(\tau_i)\}) = \mathrm{Tr}_c\Big\langle \mathcal{T} e^{-\int_0^\beta H_{\rm loc}(\tau)} O_{2n}(\tau_{2n})\cdots O_1(\tau_1)\Big\rangle_b d\tau_1\cdots d\tau_{2n}\prod_\sigma(\det M_\sigma^{-1})s_\sigma, \qquad (56)$$

where the $O_i(\tau_i)$ denote the (time-ordered) creation or annihilation operators and s_σ is 1 (-1) if the spin-σ operator with the lowest time argument is a creation (annihilation) operator. To decouple the electrons and phonons by a Lang-Firsov transformation, we rewrite the local Hamiltonian (55) as

$$H_{\rm loc} = -\mu(n_\uparrow{+}n_\downarrow) + Un_\uparrow n_\downarrow + \sqrt{2}g(n_\uparrow{+}n_\downarrow{-}1)X + \frac{\omega_0}{2}\big(X^2+P^2\big). \qquad (57)$$

Here the phonon coordinate X and momentum P, satisfying $[P,X] = i$, are related to the phonon creation and annihilation operators by $X = (b^\dagger + b)/\sqrt{2}$ and $P = i(b^\dagger - b)/\sqrt{2}$. We decouple the boson and fermion operators in $H_{\rm loc}$ by shifting X by

$$X_0 = (\sqrt{2}g/\omega_0)(n_\uparrow{+}n_\downarrow{-}1) \qquad (58)$$

using the unitary transformation e^{iPX_0}. The transformed Hamiltonian $\tilde{H}_{\rm loc} = e^{iPX_0}H_{\rm loc}e^{-iPX_0}$ becomes

$$\tilde{H}_{\rm loc} = -\tilde{\mu}(\tilde{n}_\uparrow{+}\tilde{n}_\downarrow) + \tilde{U}\tilde{n}_\uparrow\tilde{n}_\downarrow + \frac{\omega_0}{2}\big(X^2+P^2\big).$$

The first two terms of $\tilde{H}_{\rm loc}$ correspond to the local terms of the Anderson impurity model with modified chemical potential $\tilde{\mu}$ and interaction strength $\tilde{U}$, where

$$\tilde{\mu} = \mu - g^2/\omega_0, \qquad (59)$$
$$\tilde{U} = U - 2g^2/\omega_0. \qquad (60)$$

The impurity electron creation and annihilation operators are transformed to polaron operators,

$$\tilde{d}_\sigma^\dagger = e^{iPX_0}d_\sigma^\dagger e^{-iPX_0} = e^{\frac{g}{\omega_0}(b^\dagger - b)}d_\sigma^\dagger,$$
$$\tilde{d}_\sigma = e^{iPX_0}d_\sigma e^{-iPX_0} = e^{-\frac{g}{\omega_0}(b^\dagger - b)}d_\sigma.$$

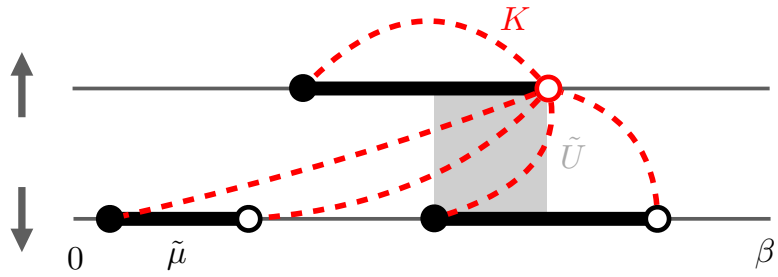

Fig. 5: *Illustration of an order $n = 3$ hybridization-expansion diagram for the Anderson-Holstein impurity model. Empty and full circles represent hybridization events. Dashed lines indicate interactions $K(\tau)$ connecting all pairs of hybridization events. We only show the lines attached to the red operator.*

After the transformation, the phonon expectation value $\langle \cdots \rangle_b$ becomes the product of a term involving electron operators, which is analogous to that computed for the Anderson impurity model without phonons, and a phonon term which is the expectation value of a product of exponentials of boson operators. The total weight of a configuration thus has the form

$$w\big(\{O_i(\tau_i)\}\big) = w_b\big(\{O_i(\tau_i)\}\big)\tilde{w}_{\text{AIM}}\big(\{O_i(\tau_i)\}\big).$$

Here, $\tilde{w}_{\text{AIM}}$ is the weight of a corresponding configuration in the Anderson impurity model with parameters modified according to Eqs. (59) and (60), while the phonon contribution is

$$w_b\big(\{O_i(\tau_i)\}\big) = \left\langle e^{s_{2n}A(\tau_{2n})}\, e^{s_{2n-1}A(\tau_{2n-1})} \cdots e^{s_1 A(\tau_1)} \right\rangle_b$$

with $0 \le \tau_1 < \tau_2 < \ldots < \tau_{2n} < \beta$, and $s_i = 1$ or (-1) if the i^{th} operator is a creation or annihilation operator. The operator in the exponent is $A(\tau) = \frac{g}{\omega_0}\big(e^{\omega_0\tau}b^\dagger - e^{-\omega_0\tau}b\big)$. The expectation value is to be taken in the thermal state of free bosons, and with the disentangling of operators $e^{X+Y} = e^X e^Y e^{-\frac{1}{2}[X,Y]}$ one finds $e^{sA(\tau)} = e^{-\frac{g^2}{2\omega_0^2}} e^{s\frac{g}{\omega_0}e^{\omega_0\tau}b^\dagger} e^{-s\frac{g}{\omega_0}e^{-\omega_0\tau}b}$, which leads to the expression

$$w_b\big(\{O_i(\tau_i)\}\big) = e^{-n\frac{g^2}{\omega_0^2}}\, e^{-\sum_{2n\ge i>j\ge 1}\frac{s_i s_j g^2}{\omega_0^2}e^{-\omega_0(\tau_i-\tau_j)}} \left\langle e^{\sum_j s_j\frac{g}{\omega_0}e^{\omega_0\tau_j}b^\dagger} e^{-\sum_j s_j\frac{g}{\omega_0}e^{-\omega_0\tau_j}b} \right\rangle_b .$$

Using $\left\langle e^{ub^\dagger} e^{vb} \right\rangle_b = e^{uv/(e^{\beta\omega_0}-1)}$ to evaluate the thermal expectation value, we finally obtain

$$w_b\big(\{O_i(\tau_i)\}\big) = \exp\left(-\frac{g^2/\omega_0^2}{e^{\beta\omega_0}-1}\left(n\big(e^{\beta\omega_0}+1\big) + \sum_{2n\ge i>j\ge 1} s_i s_j \big(e^{\omega_0(\beta-(\tau_i-\tau_j))} + e^{\omega_0(\tau_i-\tau_j)}\big)\right)\right). \quad (61)$$

This phonon contribution can be interpreted as originating from an interaction $K(\tau-\tau')$ between all pairs of operators (see Fig. 5 and Ref. [20]) of the form ($0 \le \tau \le \beta$)

$$K(\tau) = -\frac{g^2}{\omega_0^2}\frac{\cosh(\omega_0(\tau-\beta/2)) - \cosh(\omega_0\beta/2)}{\sinh(\omega_0\beta/2)}, \quad (62)$$

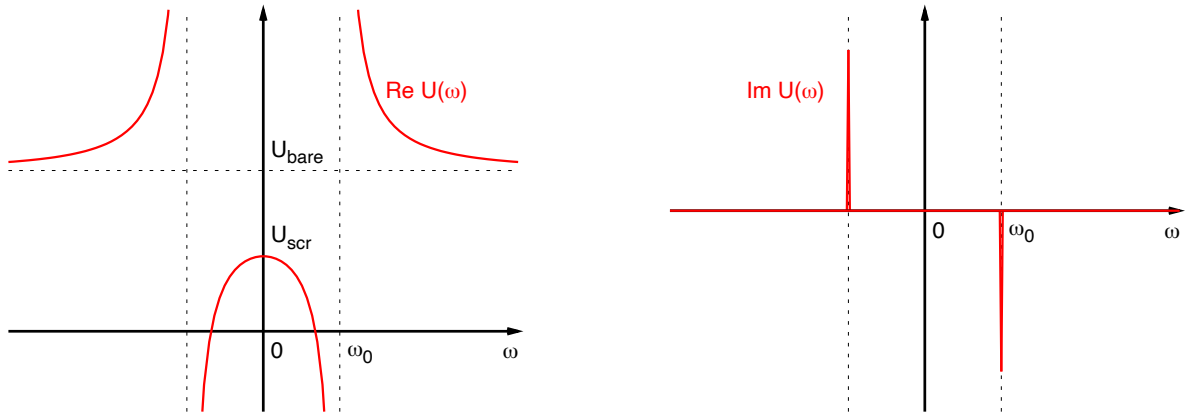

Fig. 6: *Frequency-dependent interaction $U(\omega)$ corresponding to the Anderson-Holstein impurity model with interaction $U = U_{bare}$, bosonic frequency ω_0 and electron-boson coupling g. The difference between the bare interaction U_{bare} and the screened interaction U_{scr} is $2g^2/\omega_0$ [21].*

keeping the sign factors s_i associated with creation/annihilation operators. The inclusion of phonons is thus possible without any truncation and with a negligible extra computational cost, since the computational bottleneck is the update of the determinants of hybridization functions, and not the evaluation of the nonlocal interaction between operator pairs. The phonon coupling has little effect on the average perturbation order, except very close to a bipolaronic phase.

6.2 Frequency-dependent interactions

The Anderson-Holstein impurity model corresponds to the frequency-dependent interaction $U(\omega)$ sketched in Fig. 6. In the high-frequency limit, the real part of this interaction reaches $U_{\rm bare} = U$, while the static value corresponds to the screened interaction $U_{\rm scr} = \tilde{U}$ defined in Eq. (60). The imaginary part of this frequency-dependent interaction consists of δ-functions at $\omega = \pm\omega_0$, with weight $\mp g^2\pi$ [21]. An arbitrary $U(\omega)$ can thus be thought of as arising from a Holstein-type coupling to a continuum of bosonic modes with energies ω and coupling strengths g_ω given by $g_\omega^2 = -{\rm Im}U(\omega)/\pi$. According to Eq. (62), each boson contributes an effective "interaction" $s_i s_j K(\tau_i - \tau_j) = -\frac{g_\omega^2}{\omega^2}\frac{\cosh(\omega(\beta/2-(\tau_i-\tau_j))-\cosh(\beta\omega/2)}{\sinh(\beta\omega/2)}$ between impurity creation or annihilation operators at imaginary times τ_i and τ_j. Hence, the hybridization-expansion Monte Carlo simulation for a model with general $U(\omega)$ proceeds exactly as in the case of the Anderson-Holstein impurity model, but with the K-function (62) replaced by [20]

$$K(\tau) = \int_0^\infty d\omega\, \frac{{\rm Im}U(\omega)}{\pi\omega^2}\frac{\cosh\big(\omega(\beta/2-\tau)\big) - \cosh\big(\beta\omega/2\big)}{\sinh\big(\beta\omega/2\big)} \tag{63}$$

and the shifted interaction and chemical potential (Eqs. (59) and (60)) given by

$$\tilde{\mu} = \mu + \int_0^\infty d\omega\, \frac{{\rm Im}U(\omega)}{\pi\omega}, \tag{64}$$

$$\tilde{U} = U + 2\int_0^\infty d\omega\, \frac{{\rm Im}U(\omega)}{\pi\omega} = U_{\rm scr}. \tag{65}$$

The last identity follows from the Kramers-Kronig relation and the anti-symmetry of ${\rm Im}U(\omega)$.

6.3 Boson distribution function

To measure the boson distribution function $p(x) = \big\langle \delta(x-X) \big\rangle_{\text{MC}}$, we calculate the expectation values $\big\langle \cos(\alpha X) \big\rangle_{\text{MC}}$ for different α. In order to derive the measurement formula, let us first discuss the measurement of $\langle e^{i\alpha X} \rangle_{\text{MC}}$. This measurement formula is obtained by inserting the operator $e^{i\alpha X}$ at $\tau = 0$ into the expression (56), which defines

$$w^X\big(\{O_i(\tau_i)\}\big) = \text{Tr}_c \Big\langle T_\tau e^{-\int_0^\beta H_{\text{loc}}(\tau)} O_{2n}(\tau_{2n}) \dots O_1(\tau_1) e^{i\alpha X} \Big\rangle_b \, d\tau_1 \dots d\tau_{2n} \prod_\sigma (\det M_\sigma^{-1}) s_\sigma .$$

During the Monte Carlo sampling, we then measure the ratio $w^X\big(\{O_i(\tau_i)\}\big)/w\big(\{O_i(\tau_i)\}\big)$. Since the additional $e^{i\alpha X}$ operator only modifies the bosonic factor, this amounts to measuring the ratio $w_b^X\big(\{O_i(\tau_i)\}\big)/w_b\big(\{O_i(\tau_i)\}\big)$, where $w_b^X\big(\{O_i(\tau_i)\}\big)$ is the bosonic weight factor obtained with the additional operator $e^{i\alpha X}$ at $\tau = 0$. This ratio can be expressed as

$$\begin{aligned} \frac{w_b^X\big(\{O_i(\tau_i)\}\big)}{w_b\big(\{O_i(\tau_i)\}\big)} &= \exp\left(-\frac{\alpha^2}{4}\frac{e^{\beta\omega_0}+1}{e^{\beta\omega_0}-1}\right) \\ &\quad \times \exp\left(-i\alpha X_0(\tau{=}0) - \frac{i}{e^{\beta\omega_0}-1}\sum_j s_j \frac{g}{\omega_0}\frac{\alpha}{\sqrt{2}}\big(e^{\omega_0(\beta-\tau_i)} - e^{\omega_0\tau_i}\big)\right). \end{aligned} \tag{66}$$

Note that because of the Lang-Firsov shift, this expression depends on $X_0(\tau{=}0)$, with X_0 defined in Eq. (58), and hence on the occupation of the impurity at $\tau = 0$ in the measured configuration. Since the first factor is independent of the Monte Carlo configuration, the measurement formula for $\big\langle \cos(\alpha X) \big\rangle_{\text{MC}}$ becomes

$$\begin{aligned} \big\langle \cos(\alpha X) \big\rangle_{\text{MC}} &= \exp\left(-\frac{\alpha^2}{4}\frac{e^{\beta\omega_0}+1}{e^{\beta\omega_0}-1}\right) \\ &\quad \times \left\langle \cos\Big(\alpha\sqrt{2}\frac{g}{\omega_0}\big(n_\uparrow(\tau{=}0)+n_\downarrow(\tau{=}0)-1\big) + \frac{1}{e^{\beta\omega_0}-1}\sum_j s_j \frac{g}{\omega_0}\frac{\alpha}{\sqrt{2}}\big(e^{\omega_0(\beta-\tau_i)} - e^{\omega_0\tau_i}\big)\Big)\right\rangle_{\text{MC}} . \end{aligned} \tag{67}$$

In the Monte Carlo simulation $\tilde{p}(\alpha) = \big\langle \cos(\alpha X) \big\rangle_{\text{MC}}$ is measured on a fine α-grid, which then allows to compute the boson distribution function as

$$p(x) = \frac{1}{2\pi}\int d\alpha \, \tilde{p}(\alpha) \cos(\alpha x). \tag{68}$$

References

[1] A. Georges, G. Kotliar, W. Krauth, and M.J. Rozenberg, Rev. Mod. Phys. **68**, 13 (1996)

[2] P. Werner: *Lecture notes for the International Summer School on Numerical Methods for Correlated Systems in Condensed Matter*, Sherbrooke, Canada (2008-2016)

[3] E. Gull, A.J. Millis, A.L. Lichtenstein, A.N. Rubtsov, M. Troyer, and P. Werner, Rev. Mod. Phys. **83**, 349 (2011)

[4] J.E. Gubernatis, N. Kawashima, and P. Werner: *Quantum Monte Carlo Methods* (Cambridge University Press, 2016)

[5] E. Müller-Hartmann, Z. Phys. B **74**, 507 (1989)

[6] A.N. Rubtsov, V.V. Savkin, and A.I. Lichtenstein, Phys. Rev. B **72**, 035122 (2005)

[7] E. Gull, P. Werner, O. Parcollet, and M. Troyer, Europhys. Lett. **82**, 57003 (2008)

[8] F.F. Assaad, T.C. Lang, Phys. Rev. B **76**, 035116 (2007)

[9] P. Werner, A. Comanac, L. de' Medici, M. Troyer, and A.J. Millis, Phys. Rev. Lett. **97**, 076405 (2006)

[10] L. Boehnke, H. Hafermann, M. Ferrero, F. Lechermann, and O. Parcollet, Phys. Rev. B **84**, 075145 (2011)

[11] H. Shinaoka, J. Otsuki, M. Ohzeki, and K. Yoshimi, Phys. Rev. B **96**, 035147 (2017)

[12] P. Werner and A.J. Millis, Phys. Rev. B **74**, 155107 (2006)

[13] K. Haule, Phys. Rev. B **75**, 155113 (2007)

[14] A. Läuchli and P. Werner, Phys. Rev. B **80**, 235117 (2009)

[15] E. Gull, P. Werner, A.J. Millis, and M. Troyer, Phys. Rev. B **76**, 235123 (2007)

[16] S. Fuchs, E. Gull, L. Pollet, E. Burovski, E. Kozik, T. Pruschke, and M. Troyer, Phys. Rev. Lett. **106**, 030401 (2011)

[17] B. Surer, M. Troyer, P. Werner, A.M. Läuchli, T.O. Wehling, A. Wilhelm, and A.I. Lichtenstein, Phys. Rev. B **85**, 085114 (2012)

[18] P. Werner and A.J. Millis, Phys. Rev. Lett. **99**, 146404 (2007)

[19] I.G. Lang and Y.A. Firsov, Sov. Phys. JETP **16**, 1301 (1962)

[20] P. Werner and A.J. Millis, Phys. Rev. Lett. **104**, 146401 (2010)

[21] P. Werner and M. Casula, J. Phys.: Condens. Matter **28**, 383001 (2016)